Electron impact ionization cross section of atoms

Article *in* Canadian Journal of Physics · July 2014

DOI: 10.1139/cjp-2014-0485

CITATIONS
8

READS
705

5 authors, including:

Jaspreet Kaur
Mankind Pharma Limited
72 PUBLICATIONS **272** CITATIONS
SEE PROFILE

Dhanoj Gupta
Weizmann Institute of Science
31 PUBLICATIONS **135** CITATIONS
SEE PROFILE

Rahla Naghma
The Ohio State University
36 PUBLICATIONS **219** CITATIONS
SEE PROFILE

Debdeep Ghosal
University of Basel
5 PUBLICATIONS **24** CITATIONS
SEE PROFILE

NRC Research Press

ARTICLE

Electron impact ionization cross sections of atoms

Jaspreet Kaur, Dhanoj Gupta, Rahla Naghma, Debdeep Ghoshal, and Bobby Antony

Abstract: In this article, we report the electron impact ionization cross sections for atoms Si, P, S, Sc, Cr, Mn, Co, Zn, Ga, Ge, Nb, Rh, and Cd, having applications in different areas of applied science and technology. The energy regime for the calculation is from the ionization threshold of the target to 2000 eV. We have employed the spherical complex optical potential method to calculate inelastic cross sections. A semiempirical complex scattering potential ionization contribution method is then used to estimate the ionization cross section from the inelastic cross section. In general, good agreement between the present results with available theoretical datasets and measurements are observed. The prime focus of this study was to investigate electron impact ionization phenomena in less studied targets. The results obtained are found to be quite encouraging. The values presented here are reasonable estimates of cross section for all the atoms studied.

PACS Nos.: 34.50.–s, 34.80.Bm, 34.50.Gb.

Résumé : Nous présentons ici les sections efficaces d'ionisation par impact électronique pour différents atomes, nommément Si, P, S, Sc, Cr, Mn, Co, Zn, Ga, Ge, Nb, Rh et Cd, qui trouvent des applications dans différents domaines de science et de technologie. Le domaine d'énergie des calculs va du seuil d'ionisation de l'atome jusqu'à 2000 eV. Nous utilisons le potentiel optique complexe sphérique pour calculer les sections efficaces inélastiques. Nous utilisons alors une méthode semi-empirique complexe de contributions potentiel-ionisation lors de collisions, afin d'estimer la section efficace d'ionisation à partir de la section efficace inélastique. En général, nous avons un bon accord entre nos résultats et les résultats théoriques et expérimentaux trouvés dans la littérature. L'idée première de ce travail est d'étudier les phénomènes d'ionisation par impact électronique sur des cibles moins étudiées. Les résultats obtenus sont très encourageants. Les valeurs présentées ici sont des estimés raisonnables des sections efficaces pour tous les atomes étudiés. [Traduit par le Rédaction]

1. Introduction

Study of electron collisions with atoms gives insight into the rudimentary interactions of many-electron systems. These primary physical processes analyze quantitatively the behavior of ionized gases produced by electrical discharges in lighting systems, created in fusion plasma, or found in astrophysical environments. Furthermore, the cross section data for these atoms are useful in estimating the cross sections for molecules using various additivity rules. However, the dearth of cross section data for many atomic targets is a major concern. The void in the cross section database has led us to examine the electron scattering studies of a few essential target atoms. The total ionization cross section data (Q_{ion}) calculated for the atoms investigated here are quite scarce or fragmentary. Also, they find applications in various fields of applied science.

For instance nanocrystalline silicon and silicon thin films have been implemented in many optoelectronic devices and various switching devices, which makes silicon a crucial element in the semiconductor industry [1, 2]. Silicon is also present in the sun and other stars and is also a primary component of meteorites [3]. Several phosphorous-bearing gases like P_2, PH, PH_2, PH_3, and HCP become increasingly important for the study of giant planets and dwarfs. For instance, PH_2 is found in Pegasi planets, P and PH_2 in L dwarfs, PH_2 and PH_3 in T dwarfs, and PH_3 in giant planets [4]. It has been found that the magnetosphere of Jupiter sweeps up gases and dust from its satellite Io's thin atmosphere. The atmosphere of Io contains mostly atomic and ionized sulfur, which originates from Io's volcanic eruptions. These ions are accelerated under the influence of the Jovian magnetic field and form plasma torus surrounding Io's orbit [5]. So, the ionization cross sections of silicon, phosphorous, and sulfur atoms could aid in modeling planetary atmospheres like that of Jupiter. Scandium atoms form 25 ppm of Earth's crust and its trace presence makes aluminium alloys strong. Its iodide is widely used in mercury vapor lamps by the television industry for efficient light output [6]. Chromium, produced excessively from chromite ore, finds many applications in electroplating and manufacture of non-ferrous alloys [7]. Cobalt, rhodium, and oxides of manganese and zinc have been long known for catalyzing chemical reactions [6]. Moreover, zinc and cadmium alloys are employed in corrosion protection of structural steelwork [7]. Superconducting alloys of niobium are used in MRI scanners and superconducting magnets [8]. Recently there has been intense interest and activity in the asymmetric synthesis of stereo selective organic compounds catalyzed by transition metals and its complexes, especially in the pharmaceutical industry [9]. The ionization of such catalysts can alter the outcome of any reaction.

Gallium forms various compounds like gallium nitride, gallium arsenide, and indium gallium arsenide phosphide. These are important compound semiconductors with interesting optoelectronic properties. Some of these compounds are used in solid-state devices, such as Schottky diodes, transistors, and rectifiers, and some form the basis for light-emitting diodes and semiconductor lasers. GaN nanowires have been synthesized and used in electronic and optoelectronic nanosystems [10]. Considering these facts, the study of the cross sections of these atoms becomes an important task for comprehending various electron–atom interactions.

The literature survey for the proposed atoms shows studies by Lotz [11] to calculate ionization cross sections based on a simple

Received 5 September 2014. Accepted 16 October 2014.

J. Kaur, D. Gupta, R. Naghma, D. Ghoshal, and B. Antony. Department of Applied Physics, Indian School of Mines, Dhanbad 826004, JH, India.
Corresponding author: Bobby Antony (e-mail: bka.ism@gmail.com).

empirical equation for several atoms (Z = 1–108). Bartlett and Stelbovics [12] calculated single ionization cross sections for atoms from Z = 1 to 54 using the Born approximation. They consider a Coulomb wave for the ejected continuum electron, which is made orthogonal to the occupied atomic orbitals. Other theoretical works done in the past few decades include the works of McGuire [13], Deutsch et al. [14], Kim and Stone [15], Santos et al. [16], Omidvar et al. [17], and Jha [18]. They have determined and reported various cross sections for atomic systems upon electron impact. McGuire [13] used a different variant of the Born approximation based upon expansion techniques in which the electron is contained in the Coulomb potential of variable charge. Here, the charge is approximated by a series of straight lines, which are then fitted to obtain the generalized oscillator strength for the target atom. Deutsch et al. [14] have used the semiclassical Deutsch–Märk (DM) formalism for the computation of electron impact ionization cross section of certain elements. They have obtained their parameters by fitting it to the experimental ionization cross section. Kim and Stone [15] have employed the popular binary encounter Bethe model to perform calculations on a few atoms and molecules like silicon, germanium, tin, and lead.

On the experimental front, there has been a significant contribution to electron–atom scattering research by Freund et al. [19]. They measured the ionization cross section for many atoms in different ionized states separately using a crossed-electron beam fast-atom beam method. They have measured the ionization cross section for Ga, Ge, Si, P, and S atoms. For chromium and sulfur atoms, Nelson [20] and Ziegler et al. [21] measured the ionization cross section. Tawara and Kato [22] reported experimental ionization cross sections for sulphur and zinc atoms.

In the present article, we report the total ionization cross sections (Q_{ion}) for Si, P, S, Sc, Cr, Mn, Co, Zn, Ga, Ge, Nb, Rh, and Cd atoms. The cross sections are computed using a combination of spherical complex optical potential (SCOP) formalism [23–28] and complex scattering potential – ionization contribution (CSP–ic) method [23–25]. This method has been successfully applied to many atoms previously [26–28]. The results obtained here are found to be consistent and reliable with available measurements and theoretical data.

2. Theoretical methodology

The SCOP formalism implements partial wave analysis to solve the Schrodinger equation with complex potentials as its input. The complex potential represents the electron interactions with the target atom. It contains real and imaginary parts where the real part comprises static, exchange, and polarization potentials. The role of the imaginary part is to account for the absorption losses. The complex potential is represented as

$$V_{opt}(r, E_i) = V_{st}(r, E_i) + V_{ex}(r, E_i) + V_p(r, E_i) + iV_{abs}(r, E_i) \quad (1)$$

where E_i is the incident energy, V_{st}, V_{ex}, V_p, and V_{abs} are the static, exchange, polarization, and absorption potentials, respectively. These model potentials are obtained by employing the radial charge density of the target atom and the ionization potential of the target. The parametrized Hartree–Fock wavefunctions given by Cox and Bonham [29] and Dirac–Hatree–Fock wavefunctions given by Salvat et al. [30] are used to calculate the target charge density and static potential. The exchange interactions are described by the parameter-free Hara free electron gas exchange model [31]. To include the short-range electron–electron correlation and the long-range polarization effects we use Zhang et al.'s correlation–polarization parameter-free model potential [32]. In this model, a number of multipole nonadiabatic corrections are applied, which gives a smooth and correct asymptotic form at large r. The target properties used in the calculations, such as ionization potential and polarizability, are tabulated in Table 1.

Table 1. Target properties [33].

Target	IP (eV)	α_o (Å^3)
Si	8.15	5.38
P	10.49	3.63
S	10.36	2.90
Sc	6.56	17.80
Cr	6.76	11.60
Mn	7.43	9.40
Co	7.88	7.50
Zn	9.39	5.75
Ga	5.99	8.12
Ge	7.89	6.07
Nb	6.76	15.70
Rh	7.46	8.60
Cd	8.99	7.36

The imaginary part of the complex potential is the absorption potential. The loss of incident flux into the allowed electronic excitation or ionization channels is considered by the absorption potential. The quasi-free model form of Staszeweska et al. [34] is used for the absorption potential and is given by

$$V_{abs}(r, E_i) = -\rho(r)\sqrt{\frac{T_{loc}}{2}}\left(\frac{8\pi}{10k_F^3 E_i}\right)\theta\left(p^2 - k_F^2 - 2\Delta\right)(A_1 + A_2 + A_3) \quad (2)$$

where the local kinetic energy of the incident electron is,

$$T_{loc} = E_i - (V_{st} + V_{ex} + V_p) \quad (3)$$

where A_1, A_2, and A_3 are the dynamic functions given by the following expressions:

$$A_1 = \frac{5k_F^3}{2\Delta} \qquad A_2 = -\frac{k_F^3\left(5p^2 - 3k_F^3\right)}{\left(p^2 - k_F^2\right)^2}$$

$$A_3 = 2\theta\left(2k_F^2 + 2\Delta - p^2\right)\frac{\left(2k_F^2 + 2\Delta - p^2\right)^{5/2}}{\left(p^2 - k_F^2\right)^2}$$

were $p^2 = 2E_i$ and $k_F = [3\pi^2\rho(r)]^{1/3}$ define the electron momentum and Fermi wave vector in atomic units, respectively; Δ is an energy parameter such that below this value $V_{abs} = 0$; $\theta(x)$ is the Heaviside unit step function; and I is the ionization potential of the target. In Staszeweska et al.'s model [34], Δ is assumed to be equal to I. After formulating the complex potential, the Schrödinger equation is numerically solved using the Numerov method. The solution obtained is in the form of complex phase shifts, which carry the signature of the interaction of the electron-target system. The number of partial waves needed for convergence depends on the incident electron energy. As the electron energy increases, more and more partial waves will be required for convergence.

Further, the inelasticity or the absorption factor is then calculated from the phase shifts through the relation,

$$\eta_l = \exp(-2\mathrm{Im}\ \delta_l) \quad (4)$$

The inelastic cross section [35] is then computed from the absorption factor by,

$$Q_{inel}(E_i) = \frac{\pi}{k^2}\sum_{l=0}^{\infty}(2l + 1)\left(1 - \eta_l^2\right) \quad (5)$$

The inelastic cross section takes care of all the electronic inelastic processes. Hence, the total inelastic cross section (Q_{inel}) referred to in this article is the sum of dipole-allowed electronic excitation cross sections, Q_{exc}, and the sum of all the ionization cross sections (corresponding to all ionization channels like single, double, inner shell, etc.), Q_{ion}. Thus, the present Q_{inel} can be partitioned primarily as follows:

$$Q_{inel}(E_i) = Q_{exc}(E_i) + Q_{ion}(E_i) \quad (6)$$

The first term is significant only around the threshold of excitation. Hence, Q_{exc} dies off quickly for energies above the ionization potential of the target atom. Moreover, $Q_{inel}(E_i) \geq Q_{ion}(E_i)$ with the ionization cross section being the upper limit.

Q_{inel} is not a directly measurable quantity, while Q_{ion} can be measured experimentally. So the estimation of Q_{ion} from Q_{inel} would be of great significance as it can be compared with independent experiments. Besides, Q_{ion} data are one of the necessary inputs to model various technologies and environments like plasma modeling in fusion reactors, climate modeling, and atmosphere modeling. So, we employ a semiempirical method called CSP–ic to derive Q_{ion} from Q_{inel}. This task is accomplished by defining an energy-dependent ratio of cross sections,

$$R(E_i) = \frac{Q_{ion}(E_i)}{Q_{inel}(E_i)} \quad (7)$$

such that $0 < R \leq 1$.

The ratio R is bounded by three conditions that are valid physically and are given by,

$$R(E_i) = \begin{cases} 0 & \text{for} \quad E_i \leq I \\ 1 & \text{for} \quad E_i \gg E_p \\ R_p & \text{at} \quad E_i = E_p \end{cases} \quad (8)$$

where E_p stands for the incident energy at which the calculated Q_{inel} attains its maximum. The first condition is trivial, as below the ionization threshold, the target cannot be ionized. The second condition is also physically justified, because at higher energies the excitation dies down fast and the contribution from the ionization part increases, making the ratio approach unity at incident energies much greater than the energy at the peak of inelastic cross section. However, the third condition is empirical. After pondering over various atomic [26–28] and molecular [36] targets, it is now quite well established that the contribution of ionization at the peak of inelastic cross section is around 70%–80%. The variation of R_p from 0.7 to 0.8 introduces an uncertainty of around 10% at around the peak that gradually decreases towards low and high impact energies. After examining the results obtained at various values of R_p, it was found that the cross section calculated with $R_p = 0.8$ gave consistent values for most of the atoms studied here in comparison with previous studies. Moreover, the choice of a fixed ratio makes our method reproducible, predictive, and consistent.

The functional dependence of R on energy (for $E_i \geq I$) can be expressed as,

$$R(E_i) = 1 - f(U) \quad (9)$$

For calculations, the ratio has a general analytical form,

$$R(E_i) = 1 - C_1\left[\frac{C_2}{U + a} + \frac{\ln(U)}{U}\right] \quad (10)$$

Table 2. Parameters used in (10) to find $R(E_i)$.

Target	a	C_1	C_2
Si	11.374	–1.735	–7.130
P	11.960	–1.754	–7.390
S	13.272	–1.809	–7.889
Sc	11.006	–1.728	–6.949
Cr	10.410	–1.730	–6.596
Mn	10.259	–1.737	–6.481
Co	10.943	–1.727	–6.915
Zn	11.309	–1.733	–7.100
Ga	11.720	–1.745	–7.287
Ge	11.852	–1.750	–7.344
Nb	10.414	–1.730	–6.598
Rh	12.465	–1.773	–7.593
Cd	10.636	–1.726	–6.742

Fig. 1. Electron impact ionization of silicon. Solid line, present; dashed line, Bartlett and Stelbovics [12]; dash-dot line, Kim and Stone [15]; and stars, Freund et al. [19].

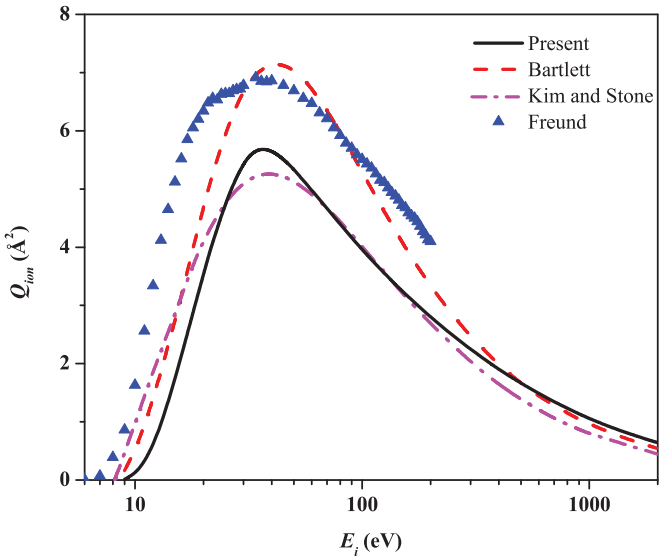

where U is a dimensionless parameter defined as $U = E_i/I$. The discrete excitation cross sections, dominated by dipole transitions, fall off as $\ln(U)/U$ at high energies. Accordingly the decrease of the function $f(U)$ must also be proportional to $\ln(U)/U$ in the high energy range. However, the two-term representation of $f(U)$ given in $U = E_i/I$ (10) is more appropriate because the first term in the bracket ensures better energy dependence at low and intermediate E_i. The parameters C_1, C_2, and a are computed by applying the boundary conditions mentioned in (8) and are given in Table 2. These parameters reflect the properties of the target under investigation. Once the ratio is known, then both Q_{ion} and Q_{exc} can be obtained using (6) and (7). Thus, the CSP–ic method gives a sufficiently good estimate of magnitude and position of the peak of the total ionization cross section. We do not claim that the result obtained here is 100% accurate, however, a reasonable estimate of the cross section within about 10% uncertainty can be estimated using this methodology.

3. Results and discussion

In this section, the Q_{ion} for Si, P, S, Sc, Cr, Mn, Co, Zn, Ga, Ge, Nb, Rh, and Cd atoms are reported from ionization threshold to 2 keV. The results are presented in graphical form in Figs. 1–13 and the cross section data are tabulated in Table 3. The data for all the

Fig. 2. Electron impact ionization of phosphorous. Solid line, present; dashed line, Bartlett and Stelbovics [12]; dash-dot line, Santos et al. [16]; and stars, Freund et al. [19].

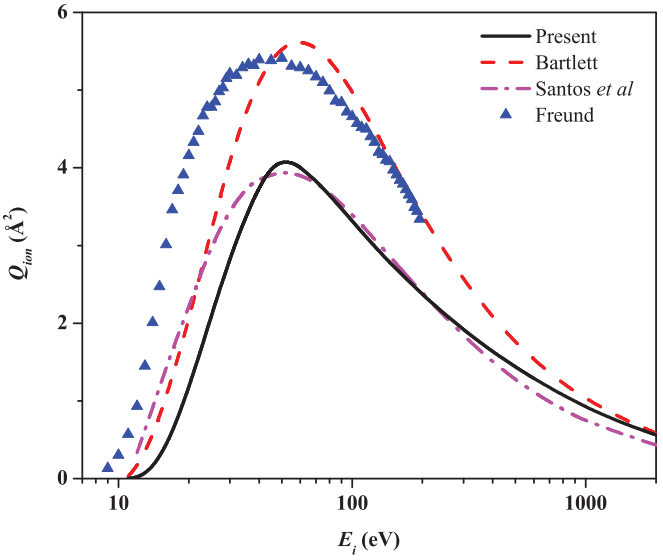

Fig. 3. Electron impact ionization of sulfur. Solid line, present; dashed line, Bartlett and Stelbovics [12]; stars, Freund et al. [19]; circles, Ziegler et al. [21]; and triangles, Tawara and Kato [22].

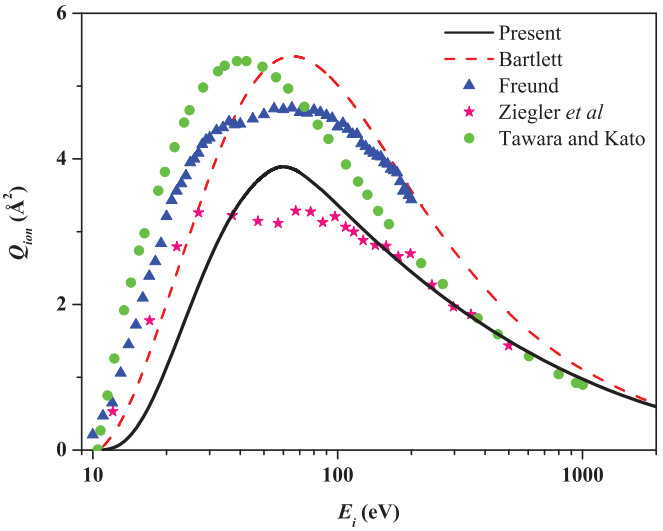

Fig. 4. Electron impact ionization of scandium. Solid line, present; dashed line, Bartlett and Stelbovics [12]; and dotted line, Lotz [11].

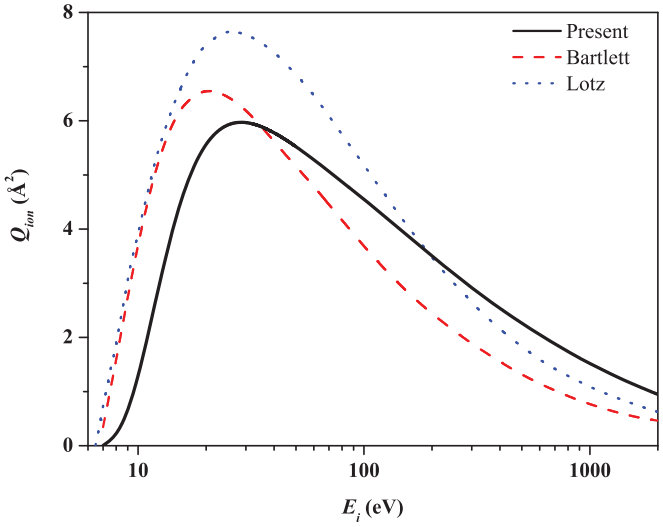

Fig. 5. Electron impact ionization of chromium. Solid line, present; dashed line, Bartlett and Stelbovics [12]; dash-dot line, DM [14]; dotted line, McGuire [13]; dash-dot-dot line, Lotz [11]; and stars, Nelson [20].

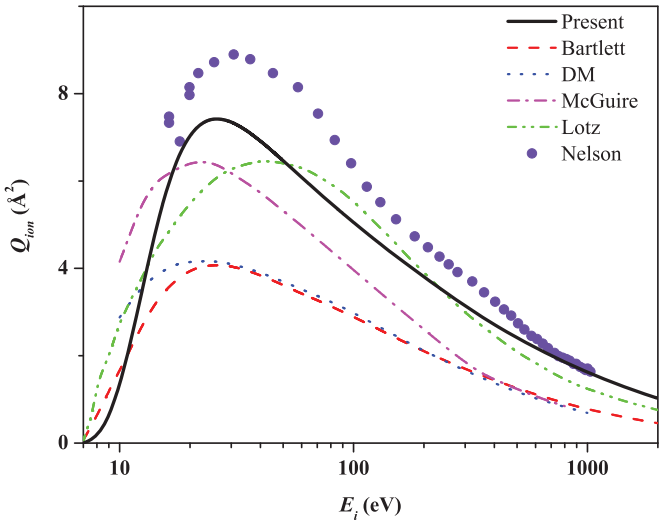

atoms are compared with previous experimental and theoretical values wherever available and are found to give a reasonable estimate of Q_{ion} in terms of shape and characteristic of the cross section curve. Finally, in Fig. 14 the correlation between maximum Q_{ion} verses the square root of the ratio of the polarizability to ionization potential for all the targets studied here is plotted to check the consistency of the reported data.

Figure 1 shows Q_{ion} for the silicon atom. The cross section of Bartlett and Stelbovics [12] overestimates present values in most of the energy region and shows good compliance with the present results only after 300 eV. However, the peak position of the present data and that of Bartlett and Stelbovics [12] falls at the same energy of around 40 eV. The cross section of Kim and Stone [15] agrees nicely with the present results throughout the given energy range. At low energies the present Q_{ion} slightly underestimates their values, around the peak the present cross section is a little higher, and beyond that the theories agree well with each other. The position of the peak is nearly the same for all the comparisons. Experimental data from Freund et al. [19] was obtained using the crossed-beam fast atom beam method. In this method, a beam of neutral atoms was prepared by charge transfer neutralization of a mass-selected ion beam and then ionized by an electron beam. This neutralization produces atoms not only in the ground state but also in the Rydberg states. It is apparent from Fig. 1 that Freund et al.'s [19] cross sections begin at energies below the ionization threshold. This is because the target gas may contain metastable atoms in some ratio while performing the experiment. Hence the experimental data of Freund et al [19] are bound to start at energies less than the ionization threshold of the target with higher cross section than the present results due to the low ionization potential of metastable atoms.

Fig. 6. Electron impact ionization of manganese. Solid line, present; and dashed line, Bartlett and Stelbovics [12].

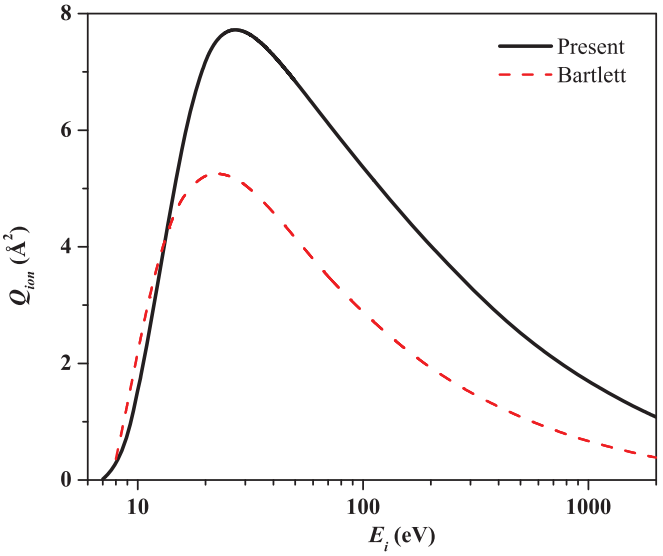

Fig. 7. Electron impact ionization of cobalt. Solid line, present; dashed line, Bartlett and Stelbovics [12]; and dash-dot line, Lotz [11].

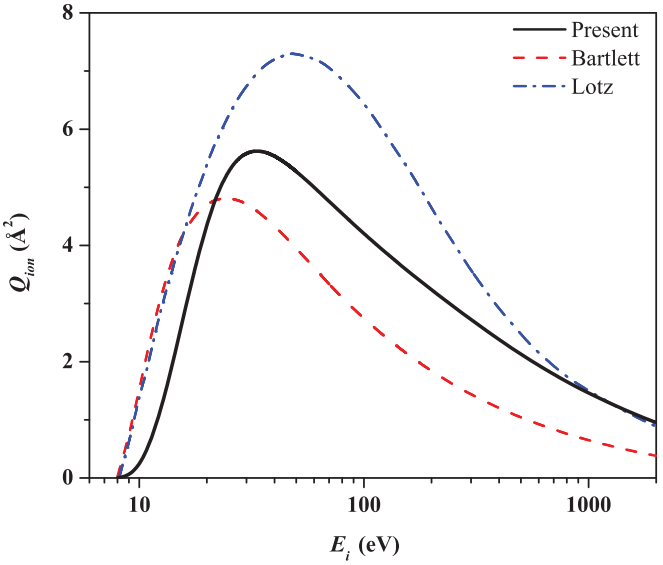

Fig. 8. Electron impact ionization of zinc. Solid line, present; dashed line, Bartlett and Stelbovics [12]; dash-dot line, DM [14]; dotted line, McGuire [13]; dash-dot-dot line, Omidvar et al. [17]; and stars, Tawara and Kato [22].

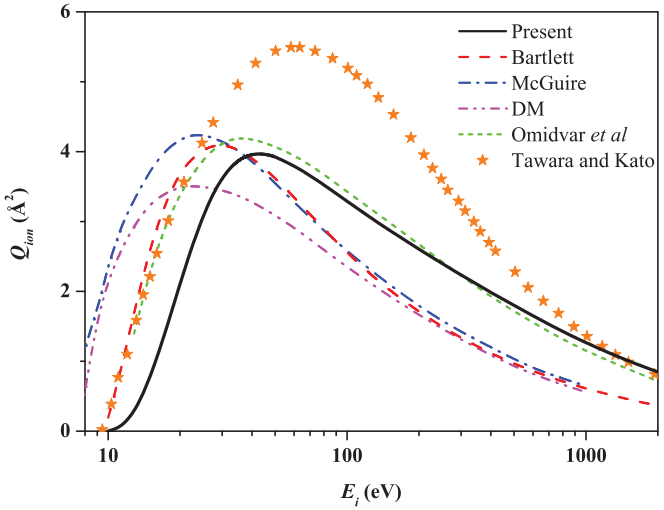

Fig. 9. Electron impact ionization of gallium. Solid line, present; dashed line, Bartlett and Stelbovics [12]; dash-dot line, DM [37]; dotted line, Lotz [11]; dash-dot-dot line, Jha [18]; and stars, Freund et al. [19].

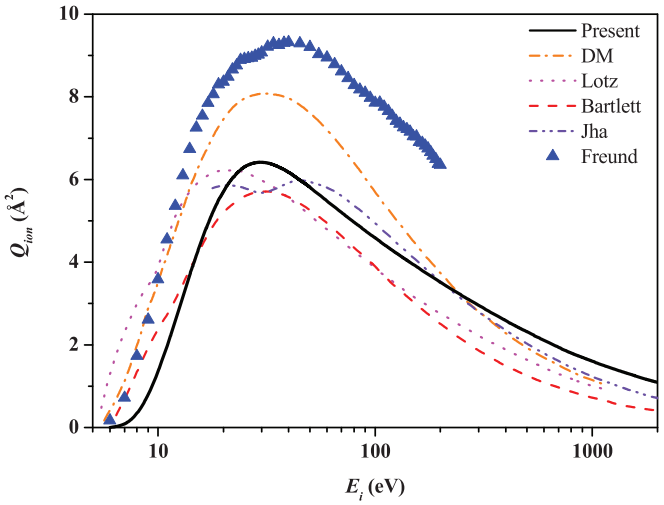

Figure 2 shows the results for the electron impact ionization of phosphorous atoms. The present results are in reasonable agreement with Santos et al. [16] throughout the compared energy range. The present ionization curve for K shows a similar shape to that of Bartlett and Stelbovics [12] including the peak position. However, the present calculated values significantly underestimate their results. The experimental data of Freund et al. [19] is higher than all other data from threshold to peak. This nature is expected, as explained in case of the silicon atom. Although the ionization peak for all the theories lies at around the same energy, the experimental peak lies at the lower energy side.

Figure 3 represents Q_{ion} of the sulfur atom. Present results are in very good accord with the measurements of Ziegler et al. [21] at high energies. However, around the peak of the ionization curve, present data overestimates the experimental values [21]. The agreement between the present results and those of Bartlett and Stelbovics [12] is quite similar to that shown in the previous case of phosphorous. The measurements reported by Tawara and Kato [22] are slightly shifted towards the lower energy side at around the peak and are higher than all reported values near and below the peak. The results of Freund et al. [19] are substantially higher than the present results throughout the energy range; however, the positions of the peak of all previous results except Kato and Tawara [22] are close to each other.

Figure 4 shows the comparison of Q_{ion} for e-scandium scattering with the available comparisons. Only theoretical data are available for comparison for this atom, which are presented by Bartlett and Stelbovics [12] and Lotz [11]. The peak position for the present data lies approximately at the same energy as that of Lotz [11], however, at high energies, their data underestimate the present values. The position of the peak of Bartlett and Stelbovics [12] is slightly left-shifted and thereafter falls rapidly below the pres-

Fig. 10. Electron impact ionization of germanium. Solid line, present; dashed line, Bartlett and Stelbovics [12]; dash-dot line, Kim and Stone [15]; and stars, Freund et al. [19].

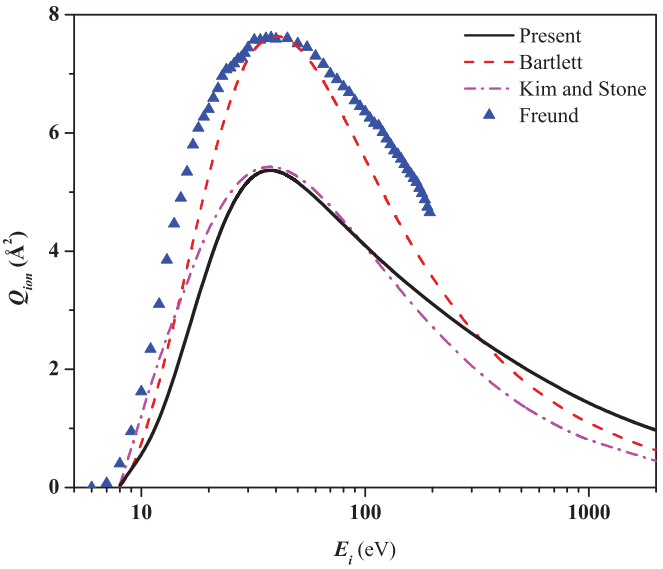

Fig. 11. Electron impact ionization of niobium. Solid line, present; and dashed line, Bartlett and Stelbovics [12].

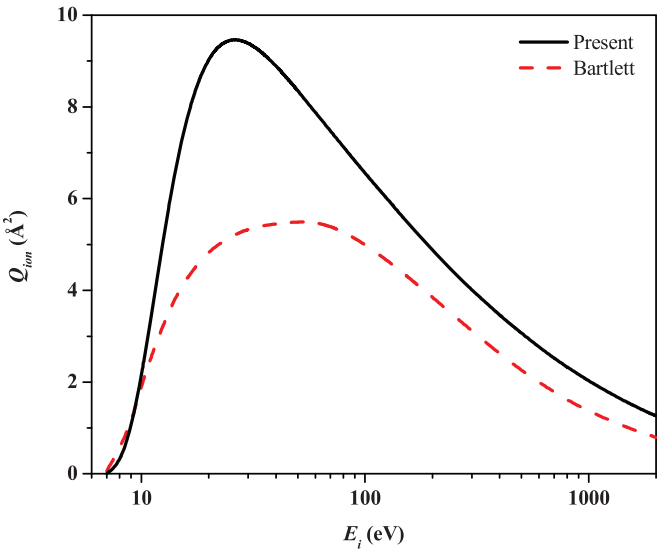

Fig. 12. Electron impact ionization of rhodium. Solid line, present; and dashed line, Bartlett and Stelbovics [12].

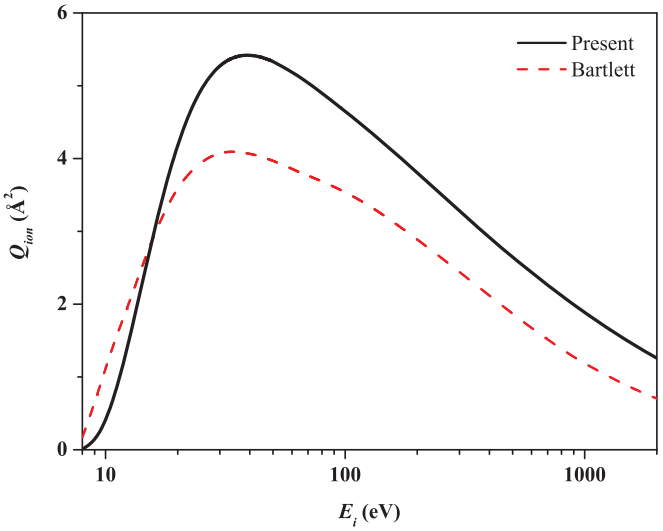

Fig. 13. Electron impact ionization of cadmium. Solid line, present; dashed line, Bartlett and Stelbovics [12]; dash-dot line, DM [14]; and dotted line, McGuire [13].

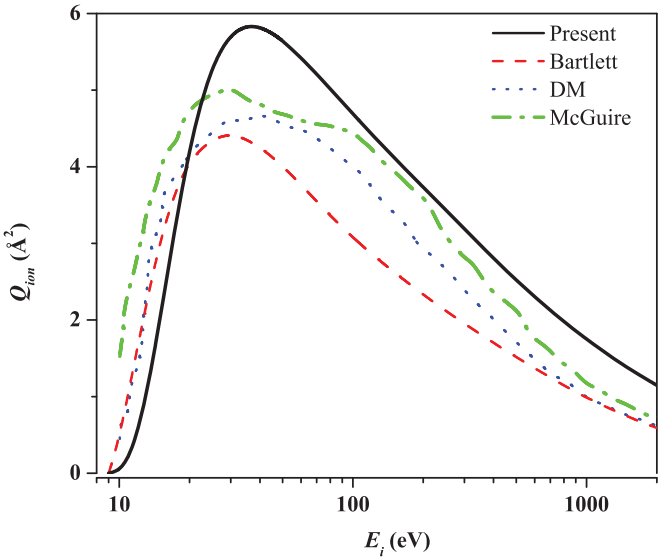

ent ionization curve. There is no experimental result available for e-Sc scattering, so it would be interesting to see experimental results along with the available theories.

Figure 5 represents the comparison of Q_{ion} for e-Cr scattering with the available experimental and theoretical cross sections. The peak position is a crucial parameter in an ionization curve. The correct positioning of the peak depends on the correct representation of the target charge density. Our results show very close agreement with the measurements of Nelson [20] in terms of shape and magnitude of the cross section. For chromium, all the other theories of Bartlett and Stelbovics [12], DM [14], McGuire [13], and Lotz [11] have nearly the same peak position. The present data are also in good accord with Lotz [11] at both low and high energies. Theoretical data of McGuire [13] are constantly lower than the present results throughout the energy range and suddenly drop after the peak compared to the experimental data of Nelson [20] and the present ones. The theoretical values of Deutsch et al. [14] are good at low energies, but the peak is shifted to the left, and so the whole curve is shifted left compared to other reported data sets [11–13, 20]. Bartlett and Stelbovics's [12] cross section is less than half the measurements, all other theories, and the present data. From the ionization curve, it is clear that cross section data of all theories are quite low in magnitude as compared to experimental and present values. Thus our results can be considered viable for practical applications.

Figure 6 shows the comparison of electron impact ionization of the manganese atom with the only available theoretical cross sectional data of Bartlett and Stelbovics [12]. There is good agreement with Bartlett and Stelbovics's [12] data up to 15 eV, however, the position of the peak is left-shifted and then the ionization curve falls rapidly beyond the peak thus underestimating the

Table 3. Q_{ion} for all the atoms studied (Å^2).

E_i (eV)	Si	P	S	Sc	Cr	Mn	Co	Zn	Ga	Ge	Nb	Rh	Cd
7	—	—	—	0.01	—	—	—	—	0.05	—	—	—	—
8	—	—	—	0.17	0.13	0.09	—	—	0.31	0.03	0.22	0.01	—
9	0.01	—	—	0.62	0.59	0.50	0.04	—	0.77	0.30	0.99	0.12	—
10	0.11	—	—	1.27	1.31	1.16	0.22	—	1.34	0.55	2.11	0.39	0.03
12	0.61	0.02	0.02	2.71	3.07	2.82	0.96	0.15	2.58	1.16	4.54	1.24	0.55
14	1.35	0.16	0.17	3.88	4.68	4.42	1.93	0.53	3.70	1.88	6.47	2.19	1.52
16	2.14	0.44	0.44	4.70	5.85	5.68	2.89	1.05	4.58	2.59	7.75	3.02	2.57
18	2.88	0.79	0.78	5.23	6.60	6.57	3.71	1.60	5.25	3.23	8.56	3.68	3.48
20	3.53	1.18	1.13	5.57	7.04	7.14	4.35	2.10	5.72	3.78	9.03	4.18	4.20
25	4.73	2.09	1.97	5.93	7.41	7.69	5.27	3.07	6.30	4.71	9.45	4.94	5.27
30	5.42	2.82	2.62	5.97	7.35	7.69	5.58	3.61	6.42	5.18	9.39	5.27	5.70
40	5.64	3.74	3.41	5.78	6.91	7.25	5.54	3.96	6.17	5.36	8.89	5.42	5.81
50	5.33	4.07	3.78	5.52	6.47	6.76	5.27	3.93	5.81	5.16	8.35	5.33	5.64
60	4.98	4.00	3.89	5.28	6.08	6.34	5.00	3.80	5.48	4.91	7.88	5.19	5.42
70	4.67	3.83	3.81	5.06	5.76	5.99	4.76	3.66	5.20	4.66	7.48	5.04	5.21
80	4.40	3.65	3.67	4.87	5.49	5.70	4.55	3.52	4.97	4.45	7.13	4.90	5.02
90	4.16	3.47	3.51	4.70	5.26	5.45	4.36	3.40	4.76	4.26	6.82	4.77	4.84
100	3.96	3.32	3.37	4.55	5.05	5.23	4.20	3.29	4.58	4.09	6.56	4.65	4.69
150	3.25	2.74	2.81	3.94	4.30	4.44	3.62	2.88	3.94	3.49	5.56	4.17	4.12
200	2.80	2.37	2.44	3.50	3.80	3.91	3.23	2.60	3.51	3.10	4.88	3.81	3.73
300	2.25	1.92	1.99	2.92	3.14	3.23	2.72	2.24	2.95	2.61	4.01	3.28	3.19
400	1.90	1.64	1.70	2.54	2.71	2.79	2.38	1.99	2.59	2.28	3.46	2.91	2.81
500	1.66	1.44	1.50	2.26	2.41	2.48	2.13	1.80	2.32	2.05	3.07	2.65	2.52
600	1.48	1.29	1.35	2.05	2.18	2.25	1.93	1.65	2.11	1.88	2.77	2.43	2.30
700	1.34	1.17	1.23	1.88	2.00	2.07	1.78	1.53	1.94	1.73	2.53	2.26	2.13
800	1.23	1.08	1.13	1.74	1.85	1.92	1.66	1.43	1.80	1.61	2.33	2.12	1.98
900	1.14	1.00	1.05	1.62	1.73	1.79	1.55	1.34	1.70	1.52	2.17	1.99	1.86
1000	1.06	0.93	0.97	1.52	1.62	1.68	1.46	1.27	1.60	1.43	2.03	1.88	1.75
1200	0.93	0.82	0.86	1.35	1.45	1.51	1.31	1.15	1.46	1.29	1.80	1.71	1.57
1400	0.83	0.73	0.77	1.22	1.31	1.37	1.20	1.05	1.34	1.19	1.62	1.56	1.44
1600	0.76	0.66	0.70	1.11	1.20	1.25	1.10	0.97	1.24	1.10	1.48	1.44	1.32
1800	0.69	0.61	0.64	1.03	1.11	1.16	1.02	0.90	1.16	1.03	1.36	1.34	1.23
2000	0.64	0.56	0.59	0.95	1.03	1.08	0.95	0.85	1.09	0.97	1.26	1.26	1.15

Fig. 14. Correlation of maximum ionization cross section with $(\alpha/IP)^{1/2}$, where α is the polarizability and IP is the ionization potential of the target.

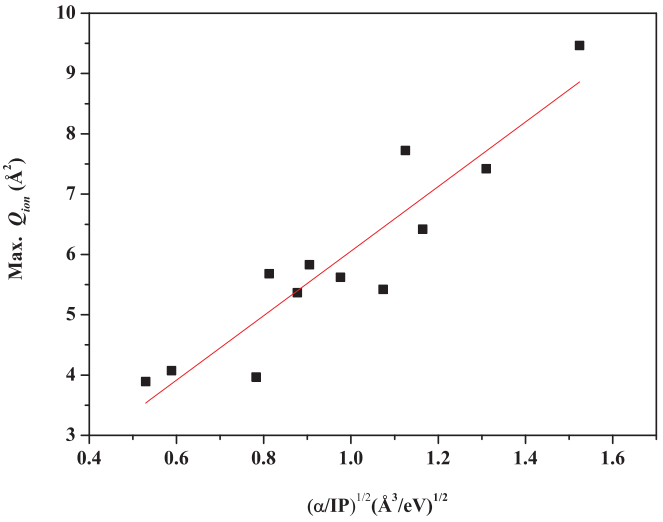

present cross sections. The shape of the curve is similar for both the theories and comparison is similar to that of the chromium atom. There are no measurements available for the e-Mn scattering. Hence, measurements on electron impact ionization of manganese can prove the reliability of the existing theories.

Figure 7 compares the Q_{ion} curve for e-cobalt scattering with the available theoretical data. The nature of the Q_{ion} curve is almost the same as that of Bartlett and Stelbovics [12] and Lotz [11]. At low energies, our data are in reasonable agreement with other theories. The peak position of Lotz [11] is slightly right shifted compared to the present data. Even at very high energies, the present data are in good accord with those of Lotz [11]. However, cross sections reported by Bartlett and Stelbovics [12] lie lower than the present data and that of Lotz [11] at the peak and for high energies. After 25 eV, their ionization curve falls rapidly. This feature of Bartlett and Stelbovics's [12] cross sectional data is observed in the case of almost all the targets studied in our work. Therefore, an experimental study of electron impact ionization of cobalt would provide a clear understanding of the variation of present theories.

In Fig. 8, we have compared our Q_{ion} for e-Zn scattering with the other theoretical and experimental data. Tawara and Kato's [22] cross section measurements exhibit a similar shape to that of the present ionization curve. The peak of present Q_{ion} lies very close to the experimental maximum value. All the available theoretical data show disagreement with each other at low energies. Moreover, the position of the peak is also different for all the theoretical comparisons. This discrepancy among theories is of serious concern as zinc is a crucial commercial element. The nature and shape of the present curve is similar to that of DM [14] and McGuire [13]. However, their peak positions are slightly left-shifted, beyond which the curve falls off rapidly at high energies. The theoretical data of Bartlett and Stelbovics [12] are in complete disagreement with the present result and show the same trend as those of DM [14] and McGuire [13]. The comparison of the present data with Omidvar et al. [17] beyond the peak is quite appreciable.

However, there is a difference in cross section at both low energies and the peak that is nearly 10%.

Figure 9 shows the comparison of Q_{ion} of e-Ga scattering with the available theoretical and experimental values. The peak positions for all the measurements and theories lie at the same energy. It is interesting to see that our cross section data follow a similar trend throughout the energy range, especially at low and high energies. The present data are in decent agreement in terms of nature and shape of the cross section curve with the theoretical data of DM [37]. The theoretical data of Jha [18] are in good agreement with present data except around the peak, where they are slightly lower than the present data. In contrast to the previous cases, for Ga the present Q_{ion} shows good agreement with the theoretical data of Bartlett and Stelbovics [12]. The peak position almost coincides with that predicted by the present theory and then decreases suddenly beyond the peak. Experimental data of Freund et al. [19] are in excellent agreement with present data below 30 eV, beyond which present data are lower than the experimental values. The experimental results of Freund et al. [19] are much higher than all the theories, however the shape and peak of the curve remain the same for all the reported data.

Figure 10 represents the present ionization curve for the germanium atom along with other theories and the available measurements. The cross section data for this atom are fragmentary. Present results are compared with the experimental data of Freund et al. [19] and the theoretical values of Kim and Stone [15] and Bartlett and Stelbovics [12]. The cross section data given by Kim and Stone [15] are in very good agreement with the present results. The present data also show good accord with the theoretical values of Bartlett and Stelbovics [12] at low and high electron impact energies. At energies near the ionization threshold, present data agree quite well with the experimental data of Freund et al. [19]. The position of the peak for all the results lies nearly at the same impact energy. This similar feature for all the comparisons is a good indication to carry out further investigations for this semiconducting target for electron impact studies. Moreover, the disagreement of the present data with Bartlett and Stelbovics's [12] calculations is quite similar to the disagreement of Bartlett and Stelbovics with Freund's measurements [19] for atoms studied in this work. Our data consistently lie below Freund et al.'s [19] experimental data, whereas Bartlett and Stelbovics [12] show inconsistent variation from Freund's measurements.

Figures 11 and 12 show a comparison of Q_{ion} data for niobium and rhodium atoms, respectively, with the available theoretical data. The cross section data for both the atoms is scarce. No experimental data are available for these atoms. The lone source of theoretical data available for comparison is presented by Bartlett and Stelbovics [12]. For both atoms, present results agree fairly well with their cross sections at low energies. The present peak position almost falls at the same energy as that of Bartlett and Stelbovics [12]. However, our results overestimate at the peak position and at high energies compared to those of Bartlett and Stelbovics [12]. At high incident energies, the fall of the cross section quickly beyond the peak for Bartlett and Stelbovic's [12] is a general trend observed for many atomic targets. However, the nature and shape of the curve is similar for both of the atoms, along with the present one.

Figure 13 represents the comparison of total Q_{ion} of e-Cd scattering with available theoretical cross sections. The present data shows good agreement with the Q_{ion} data of Bartlett and Stelbovics [12] and DM [14] up to 15 eV. It also shows good accord with the theoretical data of DM [14] and McGuire [13] in terms of nature and shape of the peak. Beyond the peak our data overestimates all the theoretical values. However, the peak position is mostly the same for all the theories along with the present result.

In Fig. 14, the maximum of present Q_{ion} is plotted against $(\alpha/IP)^{1/2}$ for all atoms studied in this work. Here we can see that a correlation exists between the maximum Q_{ion} and $(\alpha/IP)^{1/2}$. It is encouraging to see that all atoms except Sc, fall close to the line obtained by the linear fit between maximum Q_{ion} and $(\alpha/IP)^{1/2}$. Such correlations are important to check the reliability and consistency of the reported data.

4. Conclusion

Electron-impact ionization of many atoms has been investigated in the present study for which data are fragmentary in the literature. Many theoretical and experimental approaches have been developed over the years to give reliable cross section data to the atomic and molecular community. However, there still remains an avenue of research to produce cross section data for many systems as the cross section data for most of the systems vary remarkably. Hence there is a need for a simple method that can quantify reliable results. Here, we have used the quantum mechanical SCOP method to calculate inelastic cross sections. From the inelastic cross sections, we have obtained ionization cross sections by employing the semiempirical CSP–ic method. We have successfully employed these methods to find ionization cross sections for many other atoms previously [26–28]. In the present work computations have been done for Q_{ion} for 13 atoms: Si, P, S, Sc, Cr, Mn, Co, Zn, Ga, Ge, Nb, Rh, and Cd. The results presented in this article show reasonable agreement with the previously available values. At low energies the present Q_{ion} compares well with other theories, while at high energies our results agree relatively well with measurements for most of the atoms. Furthermore, the present results show a consistent deviation with the measurements of Freund et al. [19]. However, Bartlett and Stelbovics [12] data show inconsistent behavior with the present results and with the measurements of Freund et al. [19] for atoms Si, P, S, Ga, and Ge and also with the Moores experimental data [38] for noble gases [12]. Moreover the peak position of the present ionization cross section curve is close to the available measured and theoretical values for most of the targets studied here. Similar inconsistent variation between the Bartlett and Stelbovics [12] data with the results calculated by the present method and the measurements of Freund et al. [19] is observed for In, Sb, Sn, and Te atoms presented in our previous work [26]. In view of this, the present study is imperative because most of the previous available results show significant variation and there is lack of experimental data for most of the systems. Hence, we hope that the present study encourages other groups to investigate these targets experimentally and theoretically, especially the less-studied targets, like Mn, Rh, and Nb.

Acknowledgement

BA is pleased to acknowledge the support of this research by the Department of Science and Technology (DST), New Delhi through grant No. SR/S2/LOP–11/2013.

References

1. S.D. Brotherton, C. Glasse, C. Glaister, P. Green, F. Rohlfing, and J.R. Ayres. Appl. Phys. Lett. **84**, 293 (2004). doi:10.1063/1.1639137.
2. S. Hazra and S. Ray. Solid State Commun. **109**, 125 (1998). doi:10.1016/S0038-1098(98)00522-5.
3. WebElements. Silicon: the essentials [online]. Available from https://www.webelements.com/silicon/.
4. C. Visscher, K. Lodders, and B. Fegley, Jr. Astrophys. J. **648**, 1181 (2006). doi:10.1086/506245.
5. N.M. Schneider and F. Bagenal. *In* Io after Galileo: a new view of Jupiter's volcanic moon. Springer Praxis Books, Chichester, UK. pp. 265–286. 2007. doi:10.1007/978-3-540-48841-5_11.
6. The Wright Stuff. Uses of the first row transition metals [online]. Available from http://www.sky-web.pwp.blueyonder.co.uk/Science/TransMetalUses.htm.
7. International Cadmium Association. Cadmium [online]. Available from http://www.cadmium.org/.
8. J.L.H. Lindenhovius, E.M. Hornsveld, A. den Ouden, W.A.J. Wessel, and H.H.J. ten Kate. IEEE Trans. Appl. Supercond. **10**, 975 (2000). doi:10.1109/77.828394; C.R. Nave. HyperPhysics, Superconducting magnets. Georgia State University, Department of Physics and Astronomy. Available from http://

hyperphysics.phy-astr.gsu.edu/hbase/solids/supcon.html#c1 [accessed 25 November 2008].
9. T. Hayashi and M. Kumada. Acc. Chem. Res. **15**, 395 (1982). doi:10.1021/ar00084a003.
10. Encyclopaedia Britannica. Gallium (Ga) [online]. Available from http://www.britannica.com/EBchecked/topic/224460/gallium-Ga [updated 4 February 2014].
11. W. Lotz. Z. Phys. **232**, 101 (1970). doi:10.1007/BF01393132.
12. P.L. Bartlett and A.T. Stelbovics. Phys. Rev. A, **66**, 012707 (2002). doi:10.1103/PhysRevA.66.012707; At. Data Nucl. Data Tables, **86**, 235 (2004). doi:10.1016/j.adt.2003.11.006.
13. E.J. McGuire. Phys. Rev. A, **16**, 62 (1977). doi:10.1103/PhysRevA.16.62.
14. H. Deutsch, K. Becker, and T.D. Mark. Int. J. Mass Spectrom. **271**, 58 (2008). doi:10.1016/j.ijms.2007.10.001.
15. Y.K. Kim and P.M. Stone. J. Phys. B: At. Mol. Opt. Phys. **40**, 1597 (2007). doi:10.1088/0953-4075/40/8/011.
16. J.P. Santos and F. Parente. Eur. Phys. J. D, **47**, 339 (2008). doi:10.1140/epjd/e2008-00063-9.
17. K. Omidvar, H.L. Kyle, and E.C. Sullivan. Phys. Rev. A, **5**, 1174 (1972). doi:10.1103/PhysRevA.5.1174.
18. L.K. Jha. Pramana, **59**, 515 (2002). doi:10.1007/s12043-002-0048-x.
19. R.S. Freund, R.C. Wetzel, R.J. Shul, and T.R. Hayes. Phys. Rev. A, **41**, 3575 (1990). doi:10.1103/PhysRevA.41.3575. **35**, 578 (1987). doi:10.1103/PhysRevA.35.578.
20. A.N. Nelson. Electron impact ionization cross sections of gold, chromium and iron. Technical report AFML-TR-75-198. Massachusetts Institute of Technology, Cambridge, MA; Air Force Materials Laboratory, Wright Patterson, OH. 1976.
21. D.L. Ziegler, J.H. Newman, L.N. Goeller, K.A. Smith, and R.F. Stebbings. Planet. Space Sci. **30**, 1269 (1982). doi:10.1016/0032-0633(82)90100-3.
22. H. Tawara and T. Kato. At. Data Nucl. Data Tables, **36**, 167 (1987). doi:10.1016/0092-640X(87)90014-3.
23. A. Jain and K.L. Baluja. Phys. Rev. A, **45**, 202 (1992). doi:10.1103/PhysRevA.45.202. PMID:9906715.
24. M. Vinodkumar, A. Barot, and B. Antony. J. Chem. Phys. **136**, 184308 (2012). doi:10.1063/1.4711922. PMID:22583288.
25. M. Vinodkumar, H. Bhutadia, B. Antony, and N.J. Mason. Phys. Rev. A, **84**, 052701 (2011). doi:10.1103/PhysRevA.84.052701.
26. R. Naghma, B.N. Mahato, M. Vinodkumar, and B.K. Antony. J. Phys. B: At. Mol. Opt. Phys. **44**, 105204 (2011). doi:10.1088/0953-4075/44/10/105204.
27. D. Gupta, R. Naghma, and B. Antony. Can. J. Phys. **91**, 744 (2013). doi:10.1139/cjp-2013-0174.
28. B. Goswami, U. Saikia, R. Naghma, and B.K. Antony. Chin. J. Phys. **51**, 1172 (2013).
29. H.L. Cox and R.A. Bonham. J. Chem. Phys. **47**, 2599 (1967). doi:10.1063/1.1712276.
30. F. Salvat, J.D. Martnez, R. Mayol, and J. Parellada. Phys. Rev. A, **36**, 467 (1987). doi:10.1103/PhysRevA.36.467. PMID:9898887.
31. S. Hara. J. Phys. Soc. Jpn. **22**, 710 (1967). doi:10.1143/JPSJ.22.710.
32. X. Zhang, J. Sun, and Y. Liu. J. Phys. B: At. Mol. Opt. Phys. **25**, 1893 (1992). doi:10.1088/0953-4075/25/8/021.
33. R. Lide. *In* CRC handbook of chemistry and physics. CRC Press, Boca Raton, FL. 2003.
34. G. Staszewska, D.W. Schwenke, D. Thirumalai, and D.G. Truhlar. Phys. Rev. A, **28**, 2740 (1983). doi:10.1103/PhysRevA.28.2740.
35. C.J. Joachain. Quantum collision theory. North-Holland, Amsterdam. 1983.
36. M. Vinodkumar, K.N. Joshipura, C.G. Limbachiya, and B.K. Antony. Eur. Phys. J. D, **37**, 67 (2006). doi:10.1140/epjd/e2005-00257-7.
37. D. Margreiter, H. Deutsch, and T.D. Märk. Int. J. Mass Spectrom. Ion Processes, **139**, 127 (1994). doi:10.1016/0168-1176(94)90024-8.
38. D.L. Moores. Nucl. Instrum. Methods Phys. Res., Sect. B, **179**, 316 (2001). doi:10.1016/S0168-583X(01)00581-X.